



Hot and cold phonons in electrically biased grapheneWen-Hao Mao, Man-Yu Shang, and Jing-Tao Lü ^{*}*School of Physics, Institute for Quantum Science and Engineering, and Wuhan National High Magnetic Field Center, Huazhong University of Science and Technology, Wuhan 430074, China* (Received 16 June 2022; revised 29 August 2022; accepted 30 August 2022; published 7 September 2022)

Based on first-principles calculations and semiclassical transport theory, we study the nonequilibrium phonon distribution in graphene in the presence of electrical current. In addition to the hot-phonon effect, we observe a cooling of phonon modes at the same time. Interestingly, the presence of electric current along the direction connecting K and K' valleys induces an opposite dipolelike temperature distribution in the two valleys and at the Γ point. This leads to a “high-order” valley polarization of phonon distribution between K and K' . Based on the nonequilibrium phonon distribution, we furthermore study their effect on the lattice parameters and find a negative current-induced expansion coefficient. Similar to graphene’s negative thermal expansion, this is rooted in the dominant contribution of out-of-plane acoustic phonons, which do not couple directly to electrons, but gain energy from in-plane phonons through anharmonic scattering.

DOI: [10.1103/PhysRevB.106.125406](https://doi.org/10.1103/PhysRevB.106.125406)**I. INTRODUCTION**

Recent interest in two-dimensional (2D) materials has triggered intense study on the interaction between electrons and phonons and the resulting mutual energy transfer when the electronic system is driven to nonequilibrium by light [1–5], electrical current [6–9], or other types of stimuli. A two-temperature model (TTM) has been widely used to describe energy transfer between electrons and phonons [10–12], wherein an effective electronic temperature, different from the phonon temperature, is normally assumed to describe the state of the electrons under driving. Later, a multiple temperature model was proposed to improve the two-temperature model [13–15] where phonons are divided into groups with different temperatures. This is especially important in graphene and other 2D materials [16], where the in-plane and out-of-plane motions couple weakly and one single temperature is not enough to describe the phonon subsystem.

However, there are situations where such simple models are not applicable. First, the nonequilibrium electronic system may not be described by one single effective temperature, despite the fast electron-electron relaxation process. Second, electrons may couple preferentially to certain phonon modes due to different electron-phonon coupling (EPC). For example, many works have demonstrated the existence of hot-phonon generation in graphene [8,17–21] and carbon nanotubes [6,7,22–24], which show weak acoustic phonon scattering and strong optical phonon scattering. The signature of hot optical phonons during electron transport can be directly detected by Raman scattering experiments [8,9,22–24].

A quantitative account of these mode-selective processes requires detailed information on the band structure of electrons, phonons, and their coupling, which can now be obtained from first-principles calculations at the density functional the-

ory (DFT) level [25–32]. In this paper, we use graphene as a model system to study the mode-resolved nonequilibrium distribution of a phonon system. We utilize a shifted electron distribution derived from the semiclassical Boltzmann transport equation to model current-carrying electrons driven by a static electric field. We calculate electron-phonon and anharmonic three-phonon scattering rates from DFT. Using these data as inputs, phonon rate equations describing each mode are solved self-consistently. We find highly nonuniform hot- and cold-phonon distribution (relative to the equilibrium temperature) in the Brillouin zone, which depends on the phonon branch and wave vector. In particular, we find a dipolelike temperature distribution around the Γ and K points for in-plane optical phonon branches which interact strongly with electrons.

From the nonequilibrium phonon distribution, we study the current-induced change of the graphene lattice constant. It is known that the thermal expansion coefficient of graphene in a wide temperature range is negative due to negative Grüneisen parameters of the out-of-plane acoustic (ZA) and optical (ZO) phonons. Here, current-induced heating of the lattice phonon modes results in a highly nonthermal phonon distribution. How the lattice constant responds to the nonthermal distribution is not known *a priori*. Since the ZA and ZO modes with a negative Grüneisen parameter do not couple directly to electrons, one may expect lattice expansion due to selective coupling to in-plane phonons with a positive Grüneisen parameter. In fact, we find that anharmonic coupling between in-plane and out-of-plane ZA and ZO phonons results in their temperature change. Consequently, we still get negative expansion coefficients with increasing electric field or current.

II. METHOD

From the semiclassical Boltzmann transport equation, we know that, under a small applied electric field the electron

^{*}jtl@hust.edu.cn

distribution shifts along the field direction as

$$f_{\mathbf{k}} = \frac{1}{\exp\{\beta[\varepsilon_{\mathbf{k}} - (\mu + \Phi_{\mathbf{k}})]\} + 1}, \quad (1)$$

where \mathbf{k} includes the band index (n), wave vector (\mathbf{k}), spin index (s), $\varepsilon_{\mathbf{k}}$ is the electronic band energy, μ is the chemical potential without electric field, and $\beta = (k_B T)^{-1}$ is the inverse temperature with k_B the Boltzmann constant. Here we define the deviation function $\Phi_{\mathbf{k}}$ as

$$\Phi_{\mathbf{k}} = \Lambda_{\mathbf{k}}(E) \cos \theta_{\mathbf{k},\mathbf{E}}, \quad (2)$$

where $\theta_{\mathbf{k},\mathbf{E}}$ is the angle between the electron wave vector and electric field direction, and $\Lambda_{\mathbf{k}}(E)$ has a dimension of energy and is proportional to the magnitude of electric field E . From the semiclassical transport theory, we have

$$\Lambda_{\mathbf{k}}(E) = -|e|E v_{\mathbf{k}} \tau_{\mathbf{k}}, \quad (3)$$

where e is the electron charge, $v_{\mathbf{k}}$ is the electron group velocity, and $\tau_{\mathbf{k}}$ is the relaxation time. Here, due to the linear dispersion of graphene, the magnitude of group velocity does not depend on \mathbf{k} . If we furthermore ignore the \mathbf{k} dependence of $\tau_{\mathbf{k}}$ near the chemical potential, $\Lambda_{\mathbf{k}}(E)$ will not depend on \mathbf{k} . We use this approximation in this work and take $\Lambda(E)$ as a parameter to characterize the magnitude of the electric field. For weakly doped graphene, $v_{\mathbf{k}} \sim 10^6$ m/s, for $\tau_{\mathbf{k}} \sim 10^{-12}$ s, $\Lambda(E) = 1$ meV represents an electric field of 1 kV/m. The corresponding electrical current density is then obtained from the nonequilibrium distribution $\mathbf{j} = 2eV_0^{-1} \sum_{\mathbf{k}} v_{\mathbf{k}} f_{\mathbf{k}}$, where V_0 is the volume of the unit cell and 2 is for the spin degeneracy.

A. Electron-phonon scattering

The Fermi golden rule can be used to calculate the scattering rate and phonon linewidth. For electron-phonon scattering we have

$$\Gamma_{\text{ep}} = \frac{4\pi}{\hbar} \sum_{m'\mathbf{k}} |M_{m'}^{\lambda}(\mathbf{k}, \mathbf{q})|^2 (f_{\mathbf{k}} - f_{\mathbf{k}+\mathbf{q}}) \times \delta(\varepsilon_{\mathbf{k}} + \hbar\omega_{\mathbf{q}} - \varepsilon_{\mathbf{k}+\mathbf{q}}), \quad (4)$$

where $M_{m'}^{\lambda}(\mathbf{k}, \mathbf{q})$ is the EPC matrix element, and $\omega_{\mathbf{q}}$ is the phonon frequency of mode \mathbf{q} . The branch index λ is included implicitly in \mathbf{q} , and electron spin degeneracy is included in the coefficient.

There are two types of electron-phonon scattering processes, corresponding to phonon emission ($\mathbf{k}' \rightarrow \mathbf{k} + \mathbf{q}$) or absorption ($\mathbf{k} + \mathbf{q} \rightarrow \mathbf{k}'$). Correspondingly, the phonon linewidth has two opposite contributions,

$$\Gamma_{\text{ep}} = B_{\text{ep}} - A_{\text{ep}}, \quad (5)$$

where A_{ep} corresponds to the phonon emission process

$$A_{\text{ep}} = \frac{4\pi}{\hbar} \sum_{m'\mathbf{k}} |M_{m'}^{\lambda}(\mathbf{k}, \mathbf{q})|^2 f_{\mathbf{k}+\mathbf{q}} (1 - f_{\mathbf{k}}) \times \delta(\varepsilon_{\mathbf{k}} + \hbar\omega_{\mathbf{q}} - \varepsilon_{\mathbf{k}+\mathbf{q}}), \quad (6a)$$

and B_{ep} corresponds to phonon absorption

$$B_{\text{ep}} = \frac{4\pi}{\hbar} \sum_{m'\mathbf{k}} |M_{m'}^{\lambda}(\mathbf{k}, \mathbf{q})|^2 f_{\mathbf{k}} (1 - f_{\mathbf{k}+\mathbf{q}}) \times \delta(\varepsilon_{\mathbf{k}} + \hbar\omega_{\mathbf{q}} - \varepsilon_{\mathbf{k}+\mathbf{q}}). \quad (6b)$$

B. Anharmonic three-phonon scattering

The phonon linewidth due to anharmonic three-phonon scattering is written similarly as [33]

$$\Gamma_{\text{pp}} = \frac{36\pi}{\hbar^2} \sum_{\mathbf{q}'\mathbf{q}''} |\Phi_{-\mathbf{q}\mathbf{q}'\mathbf{q}''}|^2 \times [(n_{\mathbf{q}'} + n_{\mathbf{q}''} + 1)\delta(\omega_{\mathbf{q}} - \omega_{\mathbf{q}'} - \omega_{\mathbf{q}''}) + (n_{\mathbf{q}'} - n_{\mathbf{q}''})\delta(\omega_{\mathbf{q}} + \omega_{\mathbf{q}'} - \omega_{\mathbf{q}''}) + (n_{\mathbf{q}''} - n_{\mathbf{q}'})\delta(\omega_{\mathbf{q}} - \omega_{\mathbf{q}'} + \omega_{\mathbf{q}''})]. \quad (7)$$

Each term in square brackets above represents a kind of scattering process in which phonon \mathbf{q} participates. Similarly, Γ_{pp} has two contributions

$$\Gamma_{\text{pp}} = B_{\text{pp}} - A_{\text{pp}}, \quad (8)$$

where A_{pp} corresponds to the emission of phonon mode \mathbf{q} ,

$$A_{\text{pp}} = \frac{36\pi}{\hbar^2} \sum_{\mathbf{q}'\mathbf{q}''} |\Phi_{-\mathbf{q}\mathbf{q}'\mathbf{q}''}|^2 \times [n_{\mathbf{q}'} n_{\mathbf{q}''} \delta(\omega_{\mathbf{q}} - \omega_{\mathbf{q}'} - \omega_{\mathbf{q}''}) + (n_{\mathbf{q}'} + 1) n_{\mathbf{q}''} \delta(\omega_{\mathbf{q}} + \omega_{\mathbf{q}'} - \omega_{\mathbf{q}''}) + n_{\mathbf{q}'} (n_{\mathbf{q}''} + 1) \delta(\omega_{\mathbf{q}} - \omega_{\mathbf{q}'} + \omega_{\mathbf{q}''})], \quad (9a)$$

and B_{pp} corresponds to absorption

$$B_{\text{pp}} = \frac{36\pi}{\hbar^2} \sum_{\mathbf{q}'\mathbf{q}''} |\Phi_{-\mathbf{q}\mathbf{q}'\mathbf{q}''}|^2 \times [(n_{\mathbf{q}'} + 1)(n_{\mathbf{q}''} + 1)\delta(\omega_{\mathbf{q}} - \omega_{\mathbf{q}'} - \omega_{\mathbf{q}''}) + n_{\mathbf{q}'}(n_{\mathbf{q}''} + 1)\delta(\omega_{\mathbf{q}} + \omega_{\mathbf{q}'} - \omega_{\mathbf{q}''}) + (n_{\mathbf{q}'} + 1)n_{\mathbf{q}''}\delta(\omega_{\mathbf{q}} - \omega_{\mathbf{q}'} + \omega_{\mathbf{q}''})]. \quad (9b)$$

C. Rate equation

To consider the effect of applied electric field and generated electrical current, we take the electron subsystem as a nonequilibrium reservoir acting on the phonon subsystem. For the case of a relatively small electric field considered in this work this approximation should be valid. However, to consider high-field transport or a strong electron-phonon interaction, the backaction of phonons on the electronic system should be taken into account, i.e., by solving the electron and phonon Boltzmann equations self-consistently. This is a challenging problem that deserves separate study and is beyond the scope of present paper [34]. Phonons experience scattering from electrons and other phonon modes simultaneously. In equilibrium, the final steady state due to scattering is the Bose-Einstein distribution. However, when the electrons are driven to nonequilibrium, the steady state distribution of phonons also deviates from the equilibrium distribution. It can

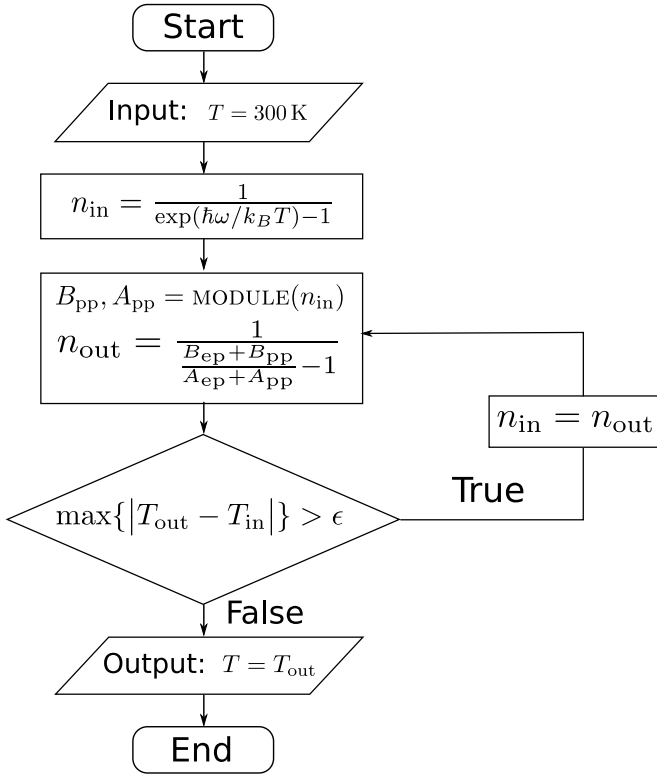


FIG. 1. The flowchart of solving rate equation. MODULE represents the code added in the PHONO3PY package to calculate A_{pp} and B_{pp} . Note that the phonon wave vector and branch indices are omitted.

be obtained from the rate equation describing the change of phonon distribution $n_{\mathbf{q}}$,

$$\frac{\partial n_{\mathbf{q}}}{\partial t} = A(n_{\mathbf{q}} + 1) - B n_{\mathbf{q}}. \quad (10)$$

Here, A and B include both electron-phonon and three-phonon scattering,

$$A = A_{ep} + A_{pp}, \quad (11)$$

$$B = B_{ep} + B_{pp}. \quad (12)$$

In steady state, the distribution function does not depend on time,

$$\frac{\partial n_{\mathbf{q}}}{\partial t} = 0. \quad (13)$$

The distribution function $n_{\mathbf{q}}$ can be determined by numerically solving Eqs. (10)–(13). Since A_{pp} and B_{pp} depend on the distribution of other phonon modes [see Eqs. (9a) and (9b)], we need to solve them self-consistently. The flowchart of the numerical procedure is shown in Fig. 1. We can define an effective temperature $T_{\mathbf{q}}$ for each mode by assuming the steady state distribution follows the Bose-Einstein form

$$T_{\mathbf{q}} = \frac{\hbar\omega_{\mathbf{q}}}{k_B \ln(1 + n_{\mathbf{q}}^{-1})}. \quad (14)$$

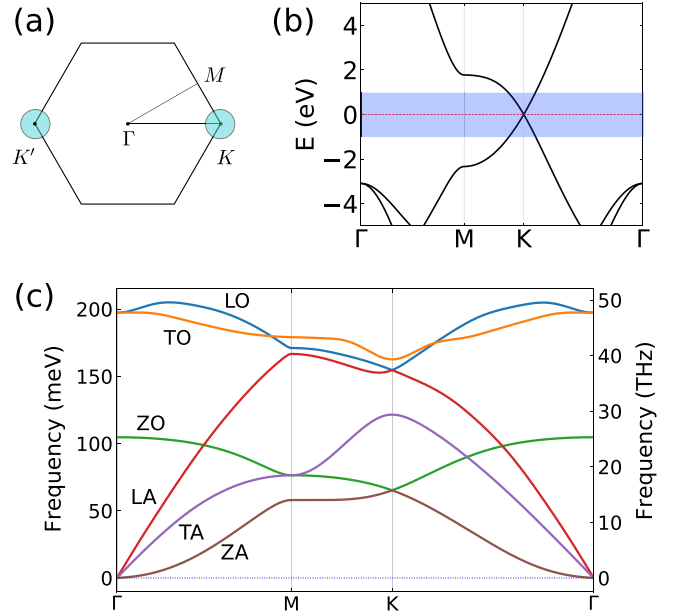


FIG. 2. (a) Brillouin zone of graphene with typical high-symmetry points. (b) Electronic band of graphene along a high-symmetry path. The light blue area shows the energy range ± 1 eV around the Fermi energy. (c) Phonon dispersion relation of graphene.

D. DFT calculation

The electron, phonon band structure, and EPC matrix elements are calculated using SIESTA [35,36] together with PHONOPY/PHONO3PY [37,38] and the INELASTICA [39] toolkit. The Perdew-Burke-Ernzerhof (PBE) version of the generalized gradient approximation (GGA) [40] is used for the exchange-correlation functional. For structure relaxation, the k -point grid used in the self-consistent-field (SCF) cycle is $45 \times 45 \times 1$. The unit cell is relaxed until the force on each atom is less than 0.001 eV/Å. We have optimized the original code of INELASTICA to improve the numerical efficiency. The scattering coefficients A_{ep} and B_{ep} in Eqs. (6a) and (6b) are computed by our own code. For the phonon calculation, second- and third-order force constants are calculated using supercells of $9 \times 9 \times 1$ and $5 \times 5 \times 1$, respectively. The mesh sampling grid in reciprocal space is $100 \times 100 \times 1$ and is gamma centered. Since the symmetry properties of phonons in the Brillouin zone are broken by an interaction with the nonequilibrium electrons, we calculate the phonon linewidth of all 10 000 q points in the Brillouin zone. In order to obtain converged results, the sampling of electronic states should be fine enough. Considering the Pauli exclusion principle and conservation of energy during electron-phonon scattering, we use 31 240 k points in two valleys K, K' [Fig. 2(a)], which is equivalent to a density of $1000 \times 1000 \times 1$ in the full Brillouin zone. These \mathbf{k} points are within 1 eV near the Fermi level, indicated by the blue area in Fig. 2(b).

III. RESULTS

A. Phonon linewidth due to electron-phonon scattering

The phonon dispersion relation of graphene is shown in Fig. 2(c). To calculate the phonon linewidth Γ_{ep} [Eq. (4)], we

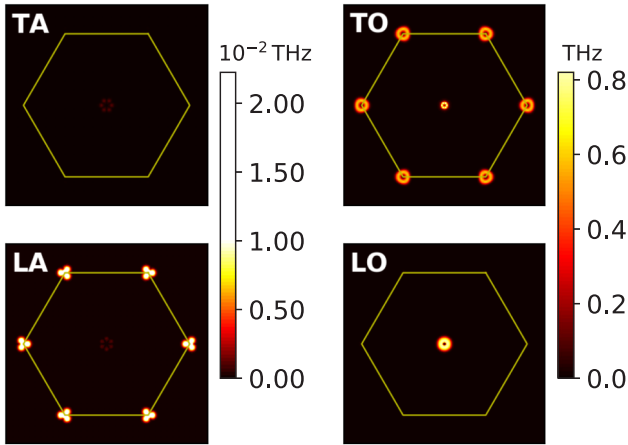


FIG. 3. Phonon linewidth due to electron-phonon scattering when electrons are in equilibrium with $T = 300$ K and $\mu = 0.3$ eV. Yellow hexagons indicate the first Brillouin zone. Note that the ZA and ZO modes do not couple directly to electrons due to mirror symmetry about the graphene plane.

set $T = 300$ K and $\mu = 0.3$ eV above the charge neutrality point. In experiments, the position of the Fermi level can be adjusted by gating. The calculated results are shown in Fig. 3. ZA and ZO modes are not shown since they do not couple directly to electrons to linear order in phonon displacement. This is due to the mirror symmetry of graphene about the 2D plane [41]. Our numerical results indeed confirm this symmetry argument. The other in-plane modes have nonzero linewidth mainly around Γ and K . Considering the electronic band structure in Fig. 2, we can attribute the phonon linewidth around Γ and K to intra- and intervalley scattering processes, respectively. Phonons outside these regions scatter much less with electrons due to the requirement of energy and crystal momentum conservation (up to integer multiples of the reciprocal lattice vector). In particular, transverse optical (TO) and longitudinal optic (LO) modes have the largest linewidth around Γ . In addition, TO modes also have a large linewidth around K . Their linewidth is an order of magnitude larger than that of transverse acoustic (TA) and longitudinal acoustic (LA) modes. These are so-called strong-coupling Γ - E_{2g} and K - A'_1 optical modes showing a strong Kohn anomaly in phonon dispersion [42,43]. This comes as no surprise since linewidth broadening and frequency renormalization are two physical effects of the EPC on the phonon properties. For acoustic branches, we observe that electrons mainly couple to the LA phonon near K . At the same time, TA and LA have a relatively weak but comparable linewidth around Γ .

B. Nonequilibrium phonon distribution in the presence of electric field

The effective phonon temperature under electrical driving at $\Lambda(E) = 29$ and 59 meV is shown in Figs. 4(a) and 4(b). The nonequilibrium electron subsystem drives phonons away from equilibrium through electron-phonon scattering. From their occupation we can assign an effective temperature to each phonon mode. For all in-plane modes, the deviation from equilibrium is the most prominent around Γ and K . This

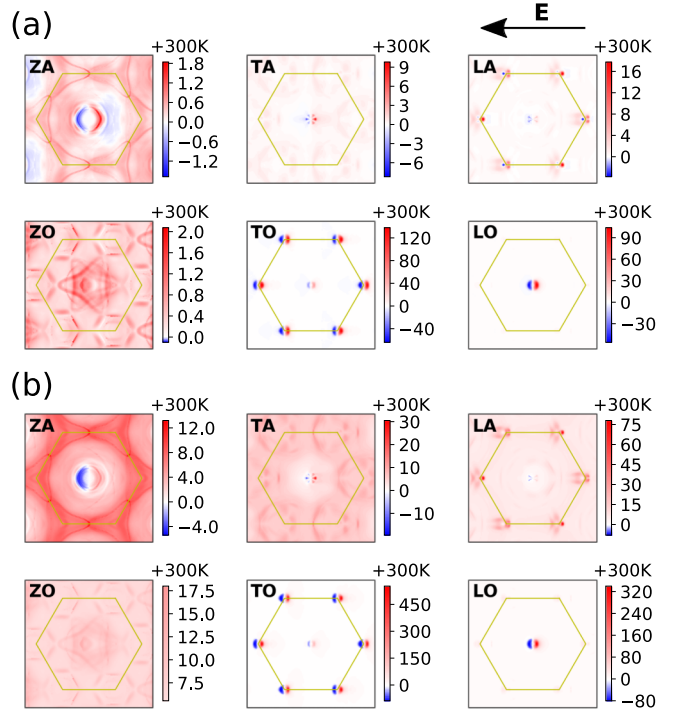


FIG. 4. Phonon effective temperature distribution under electronic drive for $\mu = 0.3$ eV, (a) $\Lambda(E) = 29$ meV and (b) 59 meV. The direction of applied electric field is indicated by the arrow in the top-right corner. The temperature in all subplots is relative to the equilibrium temperature without driving $T = 300$ K. In the ZA subplot, the small white circle at the center indicates the heat reservoir zone where ZA phonon modes are kept at 300 K during self-consistent calculation.

is consistent with the patterns of the corresponding phonon linewidth due to the electron-phonon interaction. Interestingly, in the vicinity of Γ and K , phonons are heated opposite to the electric field direction and cooled along the direction. They form dipolelike or even higher-order distribution patterns. Thus, hot and cold phonons coexist in electrically biased graphene. Although their electron-phonon coupling is negligible, ZA and ZO phonons also deviate from equilibrium considerably. This results from anharmonic phonon-phonon scattering processes, leading to energy transfer from the in-plane to out-of-plane phonon modes. Consequently, their temperature distribution within the Brillouin zone spreads out more. The corresponding temperature change is also orders of magnitude smaller than the in-plane modes.

The appearance of cold phonons under electrical drive is counterintuitive at first sight. For a better understanding of this phenomenon, we present a detailed analysis in the following. In the equilibrium case, the emission and absorption of phonons follow the principle of detailed balance. Phonon occupation is determined by the ratio between A_{ep} and B_{ep} ,

$$\frac{A_{ep}}{B_{ep}} = e^{-\beta_q \hbar \omega_q}, \quad (15)$$

with $\beta_q = 1/(k_B T_q)$. In equilibrium, T_q is the same for all phonon modes.

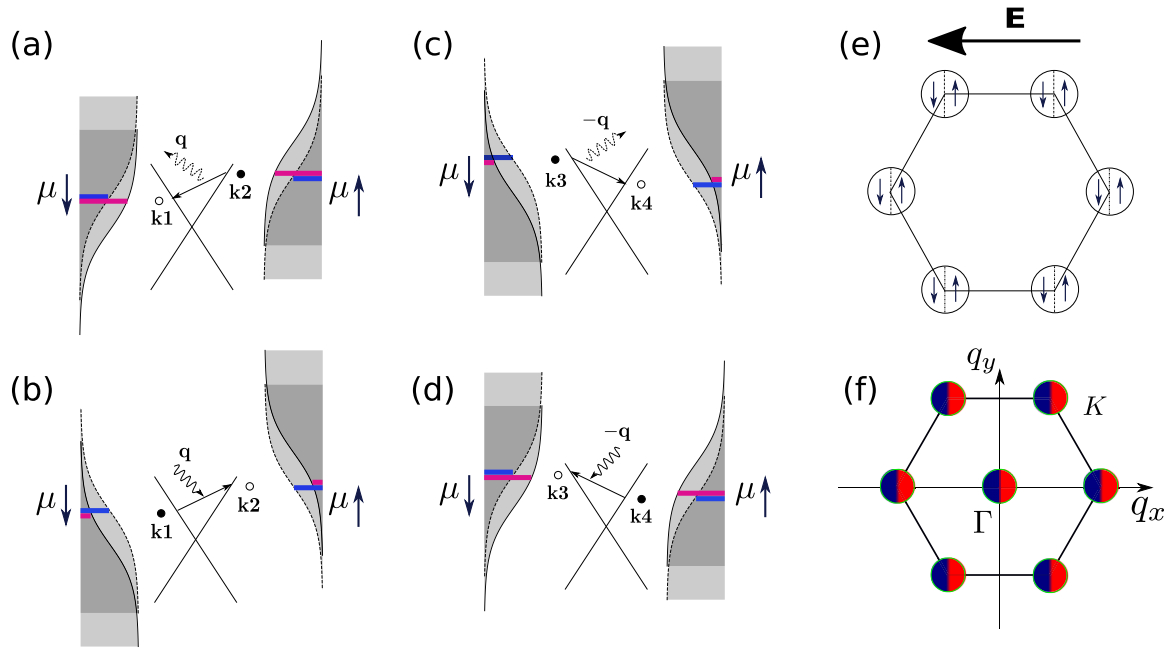


FIG. 5. Heating and cooling of phonons due to scattering with nonequilibrium electrons. (a), (b) Electron hops between \mathbf{k}_1 and \mathbf{k}_2 , accompanied by (a) emission and (b) absorption of phonon mode \mathbf{q} . Momentum and energy conservation are satisfied during the scattering process with $\mathbf{k}_1 + \mathbf{q} = \mathbf{k}_2$ and $\epsilon_{\mathbf{k}_1} + \hbar\omega_{\mathbf{q}} = \epsilon_{\mathbf{k}_2}$. Blue and red lines mark electron or hole occupation before and after electric field is applied. In (a), $f_{\mathbf{k}_2}(1 - f_{\mathbf{k}_1})$ increases because of applied electric field, leading to the enhancement of the emission rate. In (b), $f_{\mathbf{k}_1}(1 - f_{\mathbf{k}_2})$ decreases, leading to the decrease of the absorption rate. Thus phonon mode \mathbf{q} is heated. (c), (d) Similar processes as (a) and (b) lead to cooling of mode $-\mathbf{q}$. (e) The change of electron chemical potential in each valley. (f) Phonon temperature change around Γ and K .

However, when there is an external electric field, the situation is different. Focusing on one type of such scattering processes, we show in Fig. 5 the physical mechanism leading to the heating and cooling of phonon modes at the opposite wave vector. The applied electric field changes the effective chemical potential of the initial and final electronic states. This modifies the rate of phonon emission and absorption processes due to the change of the Fermi-Dirac distribution function. When the emission (absorption) process is enhanced (weakened), the corresponding phonon mode is heated. In the opposite case, the corresponding phonon mode is cooled. The details are explained in the caption of Fig. 5. The change of the electron chemical potential in each K valley is shown in Fig. 5(e). Therefore, we can easily make a schematic diagram of heating and cooling of phonons around Γ and K , as shown in Fig. 5(f). Compared with the results in Fig. 4, our simple model can qualitatively explain the phonon temperature of in-plane modes.

Moreover, in the extreme case of $A_{\text{ep}} = B_{\text{ep}}$, $T_{\mathbf{q}} \rightarrow \infty$, and when $A_{\text{ep}} > B_{\text{ep}}$, $T_{\mathbf{q}}$ is negative. This corresponds to the negative lifetime indicating phonon instability or the breakdown of the harmonic approximation. A similar effect has been predicted in molecular junctions [44]. This instability can be avoided by including anharmonic phonon scattering and calculating the coupled electron and phonon dynamics self-consistently. Since here we only consider the case of relatively weak electrical driving, we do not encounter such extreme cases.

We have calculated the total energy of each phonon branch as a function of applied electric field in Fig. 6(a). All phonon modes gain energy from the electron subsystem, including

ZA and ZO modes that do not couple directly to electrons. The energy gain of ZA and ZO modes has to be from scattering with other in-plane phonons. Thus, the energy transfer from electrons to the in-plane phonon modes, especially to the optical modes. This process is determined by EPC. In the second stage, the excess energy in the in-plane modes is further transported to out-of-plane modes via anharmonic phonon scattering. This two-stage energy transfer process is similar to that in the laser-pump experiments [17–19,21,45] and has been noticed in a related theoretical study [46]. Here, due to the shifted electron distribution, mode-selective heating and cooling of phonons take place simultaneously.

Importantly, more than 50% of the excess energy is stored in ZA and ZO modes. This seems odd at first sight. Two factors are noteworthy to understand this result. First, only LO and TO modes near Γ and K/K' couple strongly to electrons and show an obvious temperature change, while almost all ZA and ZO modes in the Brillouin zone show a temperature increase. Second, in the temperature range considered here, the heat capacity of the ZA and ZO modes is much larger than LA and TA phonon modes. Even though the temperature change of the ZA and ZO modes is much smaller, the excess energy stored in them can still be more than other branches.

C. Change of lattice constant due to nonequilibrium phonons

As has been shown by many previous works, the ZA and ZO modes of graphene have negative Grüneisen parameters contrary to the rest of the in-plane modes [47–49]. An interesting question to ask is how the graphene lattice constant

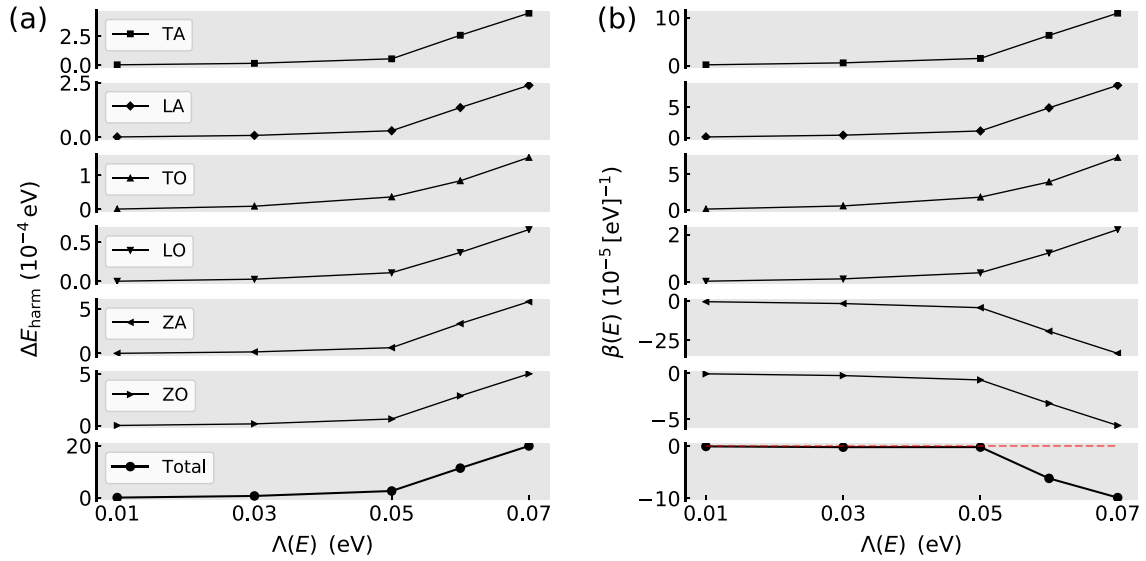


FIG. 6. (a) Change of harmonic phonon energy (per unit cell) ΔE_{harm} as a function of electric field parameter $\Lambda(E)$. (b) Dependence of electric field expansion coefficient $\beta(E)$ on $\Lambda(E)$.

changes in response to current-induced heating and cooling. The thermal expansion coefficient $\alpha(T) = V^{-1} \partial V / \partial T$ can be calculated using the Grüneisen theory [49], $\alpha(T) = (4V_0 B)^{-1} \sum_{\mathbf{q}} C_{\mathbf{q}} \gamma_{\mathbf{q}}$, where B is the bulk modulus, $C_{\mathbf{q}}$ is the mode heat capacity, and $\gamma_{\mathbf{q}}$ is the mode-resolved Grüneisen parameter. Similarly, we can define an expansion coefficient induced by electric field,

$$\beta(E) = \frac{1}{V} \frac{\partial V}{\partial E}. \quad (16)$$

Similar to $\alpha(T)$, we calculate $\beta(E)$ using

$$\beta(E) = \frac{1}{4V_0 B} \sum_{\mathbf{q}} C_{\mathbf{q}} \gamma_{\mathbf{q}} \frac{\partial T_{\mathbf{q}}}{\partial E}. \quad (17)$$

The Grüneisen parameters are obtained using the PHONOPY-QHA script [50]. The final results are shown in Fig. 6(b). We see that all modes but ZA and ZO have positive $\beta(E)$. Their absolute magnitude increases with electric field. Moreover, we find that the ZA mode contributes dominantly. This is reasonable since ZA's Grüneisen parameter is negative and much larger in magnitude than other phonons in the long-wavelength limit. Considering all the modes together, we observe a rather weak dependence of β on E for $\Lambda < 0.05$ eV, followed by a fast decrease toward the negative side. Thus, the contribution of the ZA mode remains dominant leading to negative $\beta(E)$, although they do not couple directly to electrons.

IV. CONCLUSIONS

Taking the current-carrying electron subsystem as a nonequilibrium bath for the phonon subsystem in graphene,

we have shown that hot and cold phonons are present simultaneously in the Brillouin zone. This can be explained by the opposite change of the Fermi-Dirac distribution of electronic states along and opposite to the current direction. A flowing current along the line connecting K and K' valleys leads to the high-order valley polarization of phonons between the two valleys. From these nonequilibrium distribution functions, we have shown the current-induced contraction of graphene. The physical mechanism behind this is attributed to heating of out-of-plane acoustic and optical phonons, which have negative Grüneisen parameters. Although they do not couple directly to electrons, the excess heat of in-plane phonon modes is transported to the out-of-plane modes with the help of anharmonic phonon scattering. We have taken graphene as the simplest example material. The method used here can be used to study more complicated anisotropic materials, where more interesting effects such as angular momentum generation due to valley polarization may emerge [51–53].

Finally, other consequences of the dipolelike hot- and cold-phonon distribution may also be expected. For example, one expects a corresponding phonon heat current flow along or opposite to the direction of electrical current. This represents the drag effect of nonequilibrium electrons on phonons. One can thus study the correction to the Peltier coefficient due to the electron-phonon interaction based on the results in the present paper. We will explore this problem in a future study.

ACKNOWLEDGMENTS

This work was supported by the National Natural Science Foundation of China (No. 21873033). We thank the National Supercomputing Center in Shanghai and Guangzhou for providing computational resources.

[1] I. Gierz, J. C. Petersen, M. Mitrano, C. Cacho, I. C. E. Turcu, E. Springate, A. Stöhr, A. Köhler, U. Starke, and A. Cavalleri,

Snapshots of non-equilibrium Dirac carrier distributions in graphene, *Nat. Mater.* **12**, 1119 (2013).

- [2] M. Düvel, M. Merboldt, J. P. Bange, H. Strauch, M. Stellbrink, K. Pierz, H. W. Schumacher, D. Momeni, D. Steil, G. S. M. Jansen, S. Steil, D. Novko, S. Mathias, and M. Reutz, Far-from-equilibrium electron-phonon interactions in optically excited graphene, *Nano Lett.* **22**, 4897 (2022).
- [3] C. H. Lui, K. F. Mak, J. Shan, and T. F. Heinz, Ultrafast Photoluminescence from Graphene, *Phys. Rev. Lett.* **105**, 127404 (2010).
- [4] T. Kampfrath, L. Perfetti, F. Schapper, C. Frischkorn, and M. Wolf, Strongly Coupled Optical Phonons in the Ultrafast Dynamics of the Electronic Energy and Current Relaxation in Graphite, *Phys. Rev. Lett.* **95**, 187403 (2005).
- [5] M. Breusing, C. Ropers, and T. Elsaesser, Ultrafast Carrier Dynamics in Graphite, *Phys. Rev. Lett.* **102**, 086809 (2009).
- [6] M. Lazzeri, S. Piscanec, F. Mauri, A. C. Ferrari, and J. Robertson, Electron Transport and Hot Phonons in Carbon Nanotubes, *Phys. Rev. Lett.* **95**, 236802 (2005).
- [7] M. Lazzeri and F. Mauri, Coupled dynamics of electrons and phonons in metallic nanotubes: Current saturation from hot-phonon generation, *Phys. Rev. B* **73**, 165419 (2006).
- [8] S. Berciaud, M. Y. Han, K. F. Mak, L. E. Brus, P. Kim, and T. F. Heinz, Electron and Optical Phonon Temperatures in Electrically Biased Graphene, *Phys. Rev. Lett.* **104**, 227401 (2010).
- [9] D.-H. Chae, B. Krauss, K. von Klitzing, and J. H. Smet, Hot phonons in an electrically biased graphene constriction, *Nano Lett.* **10**, 466 (2010).
- [10] M. I. Kaganov, I. M. Lifshitz, and L. V. Tanatarov, Relaxation between electrons and the crystalline lattice, *Zh. Eksp. Teor. Fiz.* **31**, 232 (1956) [*Sov. Phys. JETP* **4**, 173 (1957)].
- [11] S. I. Anisimov, B. L. Kapeliovich, and T. L. Perel'man, Electron emission from metal surfaces exposed to ultrashort laser pulses, *Zh. Eksp. Teor. Fiz.* **66**, 776 (1974) [*Sov. Phys. JETP* **39**, 375 (1974)].
- [12] P. B. Allen, Theory of Thermal Relaxation of Electrons in Metals, *Phys. Rev. Lett.* **59**, 1460 (1987).
- [13] L. Waldecker, R. Bertoni, R. Ernstorfer, and J. Vorberger, Electron-Phonon Coupling and Energy Flow in a Simple Metal beyond the Two-Temperature Approximation, *Phys. Rev. X* **6**, 021003 (2016).
- [14] S. Sadasivam, M. K. Y. Chan, and P. Darancet, Theory of Thermal Relaxation of Electrons in Semiconductors, *Phys. Rev. Lett.* **119**, 136602 (2017).
- [15] P. Maldonado, K. Carva, M. Flammer, and P. M. Oppeneer, Theory of out-of-equilibrium ultrafast relaxation dynamics in metals, *Phys. Rev. B* **96**, 174439 (2017).
- [16] M. An, Q. Song, X. Yu, H. Meng, D. Ma, R. Li, Z. Jin, B. Huang, and N. Yang, Generalized two-temperature model for coupled phonons in nanosized graphene, *Nano Lett.* **17**, 5805 (2017).
- [17] S. Butscher, F. Milde, M. Hirtschulz, E. Malić, and A. Knorr, Hot electron relaxation and phonon dynamics in graphene, *Appl. Phys. Lett.* **91**, 203103 (2007).
- [18] H. Wang, J. H. Strait, P. A. George, S. Shivaraman, V. B. Shields, M. Chandrashekar, J. Hwang, F. Rana, M. G. Spencer, C. S. Ruiz-Vargas, and J. Park, Ultrafast relaxation dynamics of hot optical phonons in graphene, *Appl. Phys. Lett.* **96**, 081917 (2010).
- [19] A. K. Vallabhaneni, D. Singh, H. Bao, J. Murthy, and X. Ruan, Reliability of Raman measurements of thermal conductivity of single-layer graphene due to selective electron-phonon coupling: A first-principles study, *Phys. Rev. B* **93**, 125432 (2016).
- [20] S. Sullivan, A. Vallabhaneni, I. Kholmanov, X. Ruan, J. Murthy, and L. Shi, Optical generation and detection of local nonequilibrium phonons in suspended graphene, *Nano Lett.* **17**, 2049 (2017).
- [21] Z. Lu, A. Vallabhaneni, B. Cao, and X. Ruan, Phonon branch-resolved electron-phonon coupling and the multitemperature model, *Phys. Rev. B* **98**, 134309 (2018).
- [22] A. W. Bushmaker, V. V. Deshpande, M. W. Bockrath, and S. B. Cronin, Direct observation of mode selective electron-phonon coupling in suspended carbon nanotubes, *Nano Lett.* **7**, 3618 (2007).
- [23] M. Oron-Carl and R. Krupke, Raman Spectroscopic Evidence for Hot-Phonon Generation in Electrically Biased Carbon Nanotubes, *Phys. Rev. Lett.* **100**, 127401 (2008).
- [24] M. Steiner, M. Freitag, V. Perebeinos, J. C. Tsang, J. P. Small, M. Kinoshita, D. Yuan, J. Liu, and P. Avouris, Phonon populations and electrical power dissipation in carbon nanotube transistors, *Nat. Nanotechnol.* **4**, 320 (2009).
- [25] R. M. Martin, *Electronic Structure: Basic Theory and Practical Methods*, 1st ed. (Cambridge University Press, Cambridge, UK, 2008).
- [26] J. Noffsinger, F. Giustino, B. D. Malone, C.-H. Park, S. G. Louie, and M. L. Cohen, EPW: A program for calculating the electron-phonon coupling using maximally localized Wannier functions, *Comput. Phys. Commun.* **181**, 2140 (2010).
- [27] F. Giustino, Electron-phonon interactions from first principles, *Rev. Mod. Phys.* **89**, 015003 (2017).
- [28] K. M. Borysenko, J. T. Mullen, E. A. Barry, S. Paul, Y. G. Semenov, J. M. Zavada, M. B. Nardelli, and K. W. Kim, First-principles analysis of electron-phonon interactions in graphene, *Phys. Rev. B* **81**, 121412(R) (2010).
- [29] F. Giustino, M. L. Cohen, and S. G. Louie, Electron-phonon interaction using Wannier functions, *Phys. Rev. B* **76**, 165108 (2007).
- [30] K. Kaasbjerg, K. S. Thygesen, and K. W. Jacobsen, Unraveling the acoustic electron-phonon interaction in graphene, *Phys. Rev. B* **85**, 165440 (2012).
- [31] T. Gunst, T. Markussen, K. Stokbro, and M. Brandbyge, First-principles method for electron-phonon coupling and electron mobility: Applications to two-dimensional materials, *Phys. Rev. B* **93**, 035414 (2016).
- [32] S. Poncé, E. Margine, C. Verdi, and F. Giustino, EPW: Electron-phonon coupling, transport and superconducting properties using maximally localized Wannier functions, *Comput. Phys. Commun.* **209**, 116 (2016).
- [33] D. C. Wallace, *Thermodynamics of Crystals* (Dover, New York, 1998).
- [34] N. H. Protik, C. Li, M. Pruneda, D. Broido, and P. Ordejón, The elphbolt ab initio solver for the coupled electron-phonon Boltzmann transport equations, *npj Comput. Mater.* **8**, 28 (2022).
- [35] J. M. Soler, E. Artacho, J. D. Gale, A. García, J. Junquera, P. Ordejón, and D. Sánchez-Portal, The SIESTA method for ab initio order-N materials simulation, *J. Phys.: Condens. Matter* **14**, 2745 (2002).
- [36] A. García, N. Papior, A. Akhtar, E. Artacho, V. Blum, E. Bosoni, P. Brandimarte, M. Brandbyge, J. I. Cerdá, F. Corsetti, R. Cuadrado, V. Dikan, J. Ferrer, J. Gale, P. García-Fernández, V. M. García-Suárez, S. García, G. Huhs, S. Illera, R. Korytár

- et al.*, SIESTA: Recent developments and applications, *J. Chem. Phys.* **152**, 204108 (2020).
- [37] A. Togo and I. Tanaka, First principles phonon calculations in materials science, *Scr. Mater.* **108**, 1 (2015).
- [38] A. Togo, L. Chaput, and I. Tanaka, Distributions of phonon lifetimes in Brillouin zones, *Phys. Rev. B* **91**, 094306 (2015).
- [39] T. Frederiksen, M. Paulsson, M. Brandbyge, and A.-P. Jauho, Inelastic transport theory from first principles: Methodology and application to nanoscale devices, *Phys. Rev. B* **75**, 205413 (2007).
- [40] J. P. Perdew, K. Burke, and M. Ernzerhof, Generalized Gradient Approximation Made Simple, *Phys. Rev. Lett.* **77**, 3865 (1996).
- [41] M. V. Fischetti and W. G. Vandenberghe, Mermin-Wagner theorem, flexural modes, and degraded carrier mobility in two-dimensional crystals with broken horizontal mirror symmetry, *Phys. Rev. B* **93**, 155413 (2016).
- [42] J. Maultzsch, S. Reich, C. Thomsen, H. Requardt, and P. Ordejón, Phonon Dispersion in Graphite, *Phys. Rev. Lett.* **92**, 075501 (2004).
- [43] S. Piscanec, M. Lazzeri, F. Mauri, A. C. Ferrari, and J. Robertson, Kohn Anomalies and Electron-Phonon Interactions in Graphite, *Phys. Rev. Lett.* **93**, 185503 (2004).
- [44] J. T. Lü, P. Hedegård, and M. Brandbyge, Laserlike Vibrational Instability in Rectifying Molecular Conductors, *Phys. Rev. Lett.* **107**, 046801 (2011).
- [45] S. Krylow, F. V. Hernandez, B. Bauerhenne, and M. E. Garcia, Ultrafast structural relaxation dynamics of laser-excited graphene: *Ab initio* molecular dynamics simulations including electron-phonon interactions, *Phys. Rev. B* **101**, 205428 (2020).
- [46] X. Yang, A. Jena, F. Meng, S. Wen, J. Ma, X. Li, and W. Li, Indirect electron-phonon interaction leading to significant reduction of thermal conductivity in graphene, *Mater. Today Phys.* **18**, 100315 (2021).
- [47] N. Mounet and N. Marzari, First-principles determination of the structural, vibrational and thermodynamic properties of diamond, graphite, and derivatives, *Phys. Rev. B* **71**, 205214 (2005).
- [48] C. Sevik, Assessment on lattice thermal properties of two-dimensional honeycomb structures: Graphene, *h*-BN, *h*-MoS₂, and *h*-MoSe₂, *Phys. Rev. B* **89**, 035422 (2014).
- [49] X.-J. Ge, K.-L. Yao, and J.-T. Lü, Comparative study of phonon spectrum and thermal expansion of graphene, silicene, germanene, and blue phosphorene, *Phys. Rev. B* **94**, 165433 (2016).
- [50] A. Togo, L. Chaput, I. Tanaka, and G. Hug, First-principles phonon calculations of thermal expansion in Ti₃SiC₂, Ti₃AlC₂, and Ti₃GeC₂, *Phys. Rev. B* **81**, 174301 (2010).
- [51] L. Zhang and Q. Niu, Angular Momentum of Phonons and the Einstein–de Haas Effect, *Phys. Rev. Lett.* **112**, 085503 (2014).
- [52] L. Zhang and Q. Niu, Chiral Phonons at High-Symmetry Points in Monolayer Hexagonal Lattices, *Phys. Rev. Lett.* **115**, 115502 (2015).
- [53] M. Hamada, E. Minamitani, M. Hirayama, and S. Murakami, Phonon Angular Momentum Induced by the Temperature Gradient, *Phys. Rev. Lett.* **121**, 175301 (2018).